An Ultrawideband System for Measuring the Dielectric Properties of Mineral Compounds in a Heat-Reaction Chamber at High Temperatures

Patrik Ottosson, Daniel Andersson, Vipin Choudhary, *Member, IEEE*, and Daniel Rönnow, *Member, IEEE*

***Abstract*— A measurement system for the measurement of microwave dielectric properties of mineral compounds at temperatures up to +1000 °C is presented. It includes the simultaneous measurement of mass and temperature. Samples' volumes in the range of 0.01–0.1 m^3 can be studied. The system comprises a heat reaction chamber on a mass scale with mounted ultrawideband (UWB) radio sensors and temperature probes. The complex refractive index is determined from the UWB signals using a technique with windowing to suppress interference and fitting of a modeled signal to the experimental ones. The developed method is validated by measuring the complex refractive index of water from +82 °C down to +23 °C and comparing with literature values. The system is used to study the calcination of limestone, i.e., the chemical decomposition of $CaCO_3$ to CaO and CO_2 when heated up to +1000 °C. The chemical decomposition is clearly seen as a decrease in mass and as significant changes in the complex refractive index. The system could also be used for other mineral compounds and other types of materials.**

***Index Terms*— Calcination, dielectric permittivity, heat chamber, high-temperature techniques, radio measurement, thermogravimetry, ultrawideband (UWB).**

I. Introduction

THE permittivity at microwave frequencies at high temperatures (100 °C–1000 °C) is important in several applications. An application is radomes used to protect antennas in airborne [1] and space [2] applications may be subject to high temperatures because of air friction. The change in permittivity with temperature changes the transmittance of radomes and hence its performance. Another example is high-temperature sensors, used in harsh environments, that harness the change in microwave permittivity with temperature [3]. Sintering of ceramics can be monitored by measuring the microwave permittivity versus temperature using a waveguide system [4]. The change in permittivity of ceramics at specific temperatures can be attributed to, e.g., crystal water turning to the gas state [5]. Water diffusion during high-temperature cycling of concrete can be observed in the microwave permittivity [6]. The microwave permittivity has been used to monitor epoxy resin during thermal curing [7]. The efficiency of microwave heating of biomass depends on the permittivity at high temperatures [8]. The resonance frequency of split ring resonator meta materials changes at high temperatures [8].

When materials, such as rocks, gravels, powder, and soil, are heated, the permittivity can change due to several factors beyond the temperature dependence of the constituting materials. The permittivity depends on chemical composition, porosity, and water content [9]. Permittivity of soil depends on moisture and temperature [10]. The chemical composition may change due to, e.g., calcination, in which case limestone is decomposed into burnt lime and carbon dioxide. The calcination is affected by porosity and chemical composition [11]. Sintering that occurs at high temperatures affects the permittivity [12].

Various techniques are used to measure the microwave permittivity at high temperatures. Microwave cavities are used [13], [14], in which case the samples are inside cavities that are heated to high temperatures. Typically, the scattering parameters (S-parameters) are measured, and the permittivity is determined using inversion methods for the specific cavity. Similarly, when waveguides are used [15], [16], the samples are inside cells that are part of the waveguide, and the permittivity is determined from the S-parameters. In free space techniques, antennas are mounted on a furnace, in which samples can be heated [17]. Using waveguide (see [18] and references therein) and cavity (see [19] and references therein) techniques, the samples' volume is typically in the range of 10–100 cm^3. Free space methods are used for larger sample volumes, typically in the order of 0.1–1 m^3. In free space methods, there is more flexibility when it comes to the sample dimensions than in cavity or waveguide techniques. However, it is more complicated to obtain data of high accuracy due to the effects of antenna near fields and radiation pattern and clutter [20].

Many substances decompose chemically when heated, which results in change in the mass. In chemistry, the technique thermogravimetry is used for the quantitative analysis of change in mass with temperature. Typically, the mass is 1 mg–1 g and temperatures up to 1600 °C are used [21], [22]. Thermogravimetric analysis combined with measurement of the temperature dependence of permittivity is reported in [23].

Manuscript received 16 December 2022; revised 27 February 2023; accepted 17 March 2023. Date of publication 12 April 2023; date of current version 24 April 2023. This work was supported by the Swedish Energy Agency. The Associate Editor coordinating the review process was Dr. Kristen M. Donnell. *(Corresponding author: Daniel Rönnow.)*

Patrik Ottosson and Daniel Andersson are with Radarbolaget, 802 67 Gävle, Sweden (e-mail: patrik.ottoson@radarbolaget.com; daniel.andersson@radarbolaget.com).

Vipin Choudhary and Daniel Rönnow are with the Department of Electronics, Mathematics and Natural Sciences, University of Gävle, 801 76 Gävle, Sweden (e-mail: vipin.choudhary@hig.se; daniel.ronnow@hig.se).

Digital Object Identifier 10.1109/TIM.2023.3265760

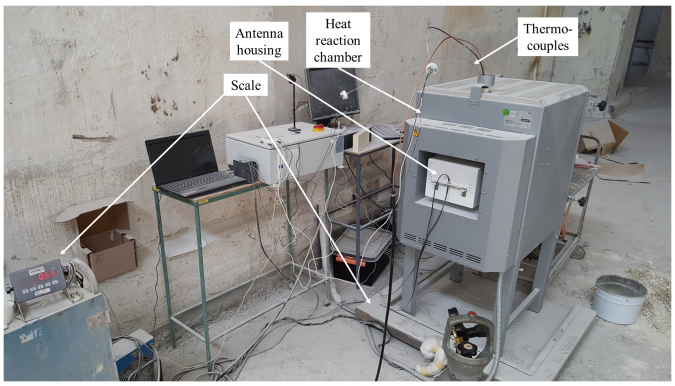

Fig. 1. Ceramic kiln or heat reaction chamber is placed on a mass scale and has thermocouples drawn through a chimney. The white box mounted on the kiln is one of the antenna housings of the UWB system.

The measurements were made separately, and the sample masses were 40 mg. In [12], the permittivity of several substances was measured during heating and the mass was measured before and after heating to record possible chemical decomposition.

Ultrawideband (UWB) radio free space techniques have found applications in in-line industrial applications. In [24], the real part of the permittivity of wood chips was measured for determining moisture content in a district heating plan. In [25], the complex permittivity was determined by a free space UWB technique that combines time and frequency domain techniques. At reheating steel furnaces, antennas and a UWB radar have been placed outside the refractory (ceramic fibers) to investigate the expansion of steel stocks at high temperatures [26].

In this article, we present a measurement system for the simultaneous measurement of the complex refractive index (or permittivity), the temperature, and the mass of samples at high temperatures. The UWB technique is equivalent to that in [24] and [25]. The system, thus, enables simultaneous thermogravimetric and permittivity measurements in heat-reaction chamber for sample volumes in the range of 0.01–0.1 m^3.

In the design of the measurement system, tradeoffs had to be made between system for measuring microwave properties, heating, temperature measurement, and weight measurements. Thus, the errors in the determined permittivity are larger than what can be achieved in waveguide and cavity measurements.

The motivation for this measurement system is threefold: 1) the simultaneous measurement of dielectric properties, temperature, and mass enables experiments, where changes in permittivity can be attributed to effects, such as chemical decomposition, dehydration, or sintering; 2) the large sample volumes make it possible to test materials used in industrial applications, where there are heterogeneous materials, such as in gravel, sand, soil, or rocks; and 3) the free space UWB technique makes it easy to transfer the system and methods to industrial in-line applications.

II. Measurement System

The presented measurement system (see Fig. 1) consists of the following:

1) a heat-reaction chamber (ceramic kiln);
2) a mass scale for gravimetric measurement;
3) thermocouples for temperature measurements; and
4) a UWB system for radio measurements.

A. Heat-Reaction Chamber

The used heat-reaction chamber is a rebuilt ceramic kiln (see Fig. 1). In our case, it is an electrically heated Nabertherm N140 ES heated from three sides (bottom and two sides). This kiln can be heated to 1300 °C and it is isolated with ceramic refractories. In general, any kind of kiln could be used for transmission radio measurement if two opposite sides of the kiln are free from metal, heating elements, and wires. It is also possible to use heat-reaction chambers heated with liquefied petroleum gas (LPG) or liquefied natural gas (LNG). The inside geometry of the Nabertherm N140 ES is 450 × 580 × 570 mm (width × depth × height).

The samples can be placed solely in the kiln, but normally, it is impractical because it may quickly destroy the heat element. Therefore, the samples of the mineral compounds are preferably placed into refractory containers. The used containers are made of alumina (Al_2O_3), which is a standard material used in heating furnaces and kilns. The width and height are 310 and 330 mm (inner dimension), respectively. The length can be 210, 310, or 410 mm. The containers must be large enough (width and height) to enable the electromagnetic waves to propagate through the container and the sample. To minimize circumferential radio signals, a metal shield for high temperatures can be placed around the containers. Preferably, the container is placed closed to the back wall (holding the transmitter or receiver) to force the electromagnetic waves to propagate through the container and the sample. Reciprocity makes the Tx and Rx positions equivalent. It is not possible to use containers that fit exactly to both walls, because the refractory material in the container and the kiln will expand and shrink independently during the heating and cooling of the kiln.

The heating cycle must be adapted to the investigated material. The heating and cooling rates in these kilns are normally 50 °C/h to minimize the damages of the kiln, such as shrinkage cracks in the refractories. The investigated materials also have a temperature response time to be considered. Larger containers contain more material and will therefore have longer temperature response time than small ones. To find a suitable heating cycle requires several iterations.

B. Mass Scale

Gravimetric measurements are performed by placing the kiln on a mass scale (see Fig. 1). In our case, the scale (Vetek Weighing AB) was purposely built and equipped with four loadcells to achieve high resolution, which is 50 g. In our setup, the highest possible load weight is 400 kg.

C. Thermocouples

Temperature measurements are carried out by using high-temperature thermocouples, which can be placed in the

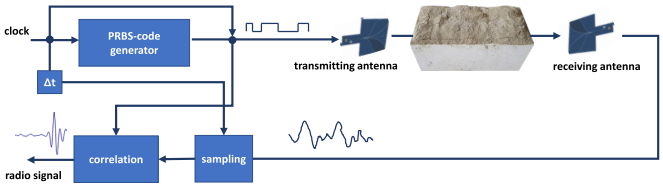

Fig. 2. Used UWB system (DiRP) uses M-sequence technology to generate the UWB signal. The antennas are Vivaldi antennas.

atmosphere and in the investigated sample and material. At temperatures above 1100 °C, thin thermocouples (2–5 mm) may hold only for one or a few experiments. Therefore, it is favorable to use thicker thermocouples (≥6 mm in diameter). The thermocouples should not have protective coatings to achieve short thermal response time. The used thermocouples (Pentronic model 8102000) are mineral-oxide-insulated, metal-sheathed (MIMS) thermocouples and can measure temperatures in the range from −200 °C to +1400 °C.

D. UWB System

The used UWB system is a proprietary M-sequence radar called digital radar processor (DiRP, developed by Radarbolaget) [24], [25], [27]. The UWB radio signal is generated by digital correlation of a pseudorandom binary sequence (PRBS)-code [28] that is transmitted and received by Vivaldi antennas (see Fig. 2). The signals are subsampled to receive higher resolution. For example, at a center frequency of 0.75 GHz, the signal will have a resolution of 0.09 ns. At 2.5 GHz, the resolution will be 0.027 ns. The resolution in measured time of flight is down to 0.002 ns. The signals can be recorded and stored several times per second at desired acquisition rate. The fastest valid measurement cycle is around 5 ms. Longer measurement times are used for averaging, to increase dynamics and system gain, and to obtain higher accuracy. Data are stored in text or binary formats, which can be uploaded and analyzed in, e.g., MATLAB, Scilab, or in a C-program. A time stamp is used to synchronize the UWB signals with data from the mass scale and the thermocouples.

Vivaldi antennas have endfire characteristics and are UWB. The used Vivaldi antennas are balanced to enhance the signal and to avoid problems with disturbances in the ground plane. The antennas are placed inside metal housings (white box in Fig. 1) to hold the antennas and to ensure directional transmitting. The antennas have a directional gain of 4 dBi; a high directional gain is valuable if the investigated material absorbs much of the radio signal. The design of the antennas is described in [29] and a radiation pattern for the different polarization states is given in [24]. Maximum effective isotropic radiated power (EIRP) from the transmitter is between −15 and −10 dBm depending on the configuration. The signal-to-noise ratio of the emitted signal is 40 dB; using correlation, the signal-to-noise ratio of the detected signal can be down to 70 dB.

In the experiments, the center frequencies of the transmitted signals were 0.75 and 2.5 GHz. The frequency spectra are approximately 0.375−1.125 GHz and 1.25−3.75 GHz, respectively. The center frequency of the used UWB-system can be set from 0.75 to 3.125 GHz. It is possible to use the same antennas with any center frequency, but for best performance, the antennas and antenna housings should be adapted to the frequency. The radio waves propagate through a container filled with a mineral compound, which filters the signal. Thus, the antennas, the transmitted signal, and the filtering in the compound determine the useful frequency band.

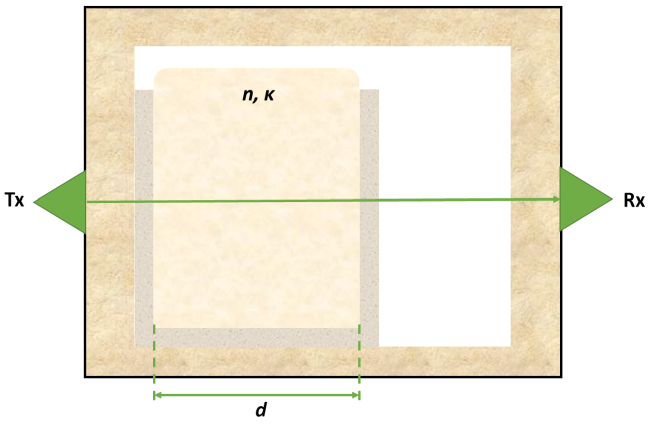

Fig. 3. Outline of the kiln with the container filled with a mineral compound with refractive index, n and κ. The transmit (Tx) and receive (Rx) antennas are indicated.

III. Permittivity Determination

We use the complex refractive index, $\underline{n} = n + j\kappa$, to describe the dielectric properties of the investigated materials. The method to retrieve material properties from experimental data is based on wave propagation theory in which $\underline{n}$ is used. The permittivity, $\varepsilon = \varepsilon' + j\varepsilon''$, is easily obtained as $\varepsilon' = n^2 - \kappa^2$ and as $\varepsilon' = 2n\kappa$.

A. Measurement Procedure

Measurements are made with the container inside the kiln (see Fig. 3). Measurements are performed in: 1) an empty kiln; 2) an empty container; and 3) a filled container. The measured signals are denoted as $y_{0e}(t)$, $y_{0c}(t)$, and $y_{1c}(t)$, respectively.

B. Signal Analysis

The time delay of the signal, $y_{0c}(t)$, is determined from the third zero-crossing before the main peak (see [24]). This time delay, τ_c, is used to compensate for the time delay of the container walls. The signal $y_{1c}(t)$ is shifted τ_c and the shifted signal is denoted as $y_{1x}(t)$.

To determine n and κ, we use the wave propagation model (a simplification of [25, eq. (26)])

$$Y_{1m}(f) = Y_{0e}(f)\cdot e^{-j2\pi f(\tau_1-\tau_o)} \cdot e^{\frac{-2\pi f d\kappa}{c_0}} \cdot d^{-\beta} \qquad (1)$$

where $Y_{0e}(f)$ and $Y_{1m}(f)$ are the Fourier transform of $y_{0e}(t)$, and the modeled signal through the sample, $y_{1m}(t)$, respectively, f is the frequency, τ_0 and τ_1 are the time delays of the reference and sample signals, respectively, d is the width of the medium (interior of container), c_0 (299, 792, and 458 m/s) is the speed of light in vacuum, and β is a path loss constant used to model the effects of finite distance between the antennas and

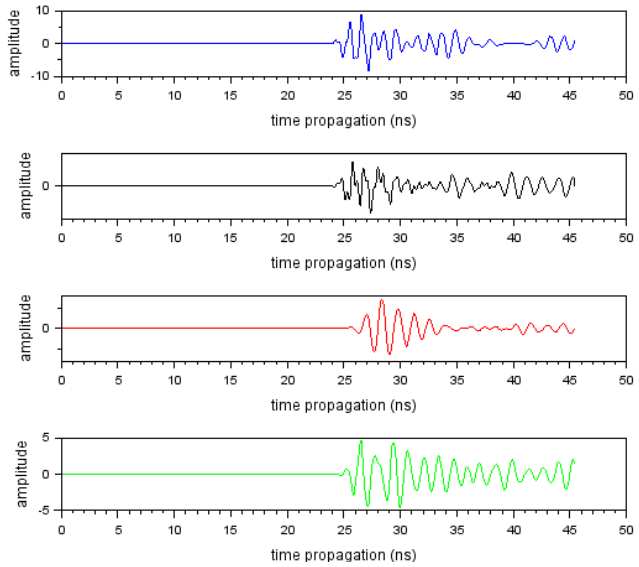

Fig. 4. Signal measured through the empty kiln, $y_{0e}(t)$, (blue), through the empty container, $y_{0c}(t)$, (black), and through two different material compounds, $y_{1c}(t)$, $CaCO_3$ (red) and CaO (green), respectively.

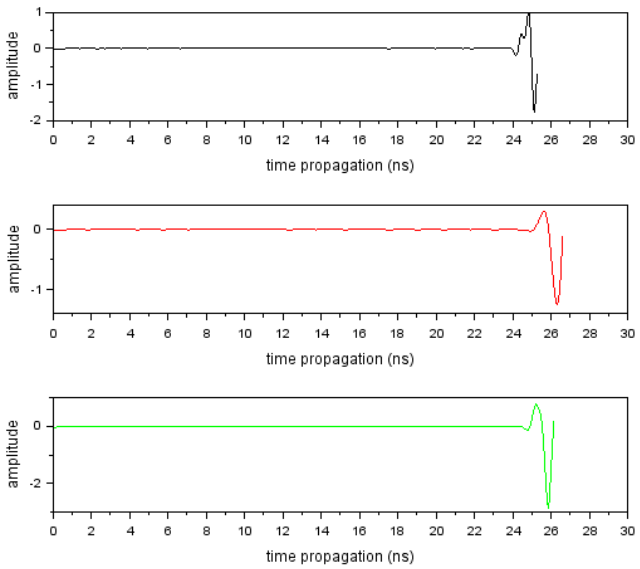

Fig. 5. First part (three zero crossings) of the UWB signals is minorly influenced by multipath interference and is selected by windowing: empty container, $w(t)y_{0c}(t)$, (black), and through mineral compounds, $z_x = w(t)y_{1x}(t)$, $CaCO_3$ (red), and CaO (green).

finite size of the container ($1 < \beta < 2$) [25]. Notice that in (1), $\tau_1 - \tau_o$ shifts the signal in time, κ attenuates and broadens the signal in time, and $d^{-\beta}$ scales the amplitude. The real part, n, is computed from the time delay, $\tau_1 - \tau_o$

$$n = \frac{c_0}{v} = \frac{d}{\tau_0} \cdot \frac{\tau_1}{d} = \frac{\tau_0 + (\tau_1 - \tau_0)}{\tau_0} = \frac{\tau_1}{\tau_0} \tag{2}$$

where v is the speed of electromagnetic waves in the medium (investigated compound).

When the signal is transmitted through an empty container or a container with mineral compound, it will be time-delayed and attenuated. The time delays, $\tau_1 - \tau_o$ (and hence n) and, κ, can be determined by using (1) to fit to $y_{1m}(t)$ to $y_{1x}(t)$ to. The determination is made in several steps. We illustrate the signals as seen at some steps by experimental data on limestones at a center frequency of 0.75 GHz (described further in the following). In Fig. 4, the reference signals, $y_{0e}(t)$ and $y_{0c}(t)$, and two examples of a signal transmitted through a mineral compound, $y_{1x}(t)$, are shown. The technique for finding the time delay and the imaginary part of the complex refractive index is as follows.

1) The Fourier transforms, $Y_{0e}(f)$ and $Y_{1x}(f)$, of the reference signal, $y_{0e}(t)$, and experiment signal, $y_{1x}(t)$, are calculated.
2) Equation (1) is used to calculate a modeled signal, $Y_{1m}(f)$, from $Y_{0e}(f)$ for different $\tau_1 - \tau_0$ and κ.
3) Using the inverse Fourier transform, the modeled signal, $y_{1m}(t)$, is calculated.
4) A rectangular time window, $w(t)$, is used on $y_{1m}(t)$; $w(t)$ is selected as the length in time that contains three zero-crossings (see Fig. 5), and the resulting signal is $z_m(t) = w(t)y_{1m}(t)$. The windowing suppresses interference from multipath propagation.
5) The window $w(t)$ is applied to $y_{1x}(t)$, resulting in $z_x(t) = w(t)y_{1x}(t)$.
6) The normalized cross correlation between $z_m(t)$ and $z_x(t)$ is calculated for each $\tau_{10} = \tau_1 - \tau_0$ and κ

$$\rho_{mx}(\tau_{10}) = \frac{r_{mx}(\tau_{10})}{\sigma_m \sigma_x}. \tag{3}$$

where $r_{mx}(\tau_{10}) = z_x(t) * z_m(-t)$ is the correlation function and $*$ denotes the convolution; σ_m and σ_x are the standard deviations of $z_m(t)$ and $z_x(t)$, respectively.
7) The highest value of ρ_{mx} gives the best fitted $\tau_1 - \tau_o$ and κ [corresponding signals, $z_m(t)$ and $z_x(t)$, in Fig. 6, also scaled by $d^{-\beta}$]. Fig. 6 also shows the reference signals $w(t)y_{0e}(t)$ and $w(t)y_{0c}(t)$, where the latter is shifted τ_c.

The frequency content will change between the reference and the experimental signals because of attenuation and multipath interference. The latter is caused by reflections in the container and kiln walls and by different propagation paths through the compounds. The first part of the signals has the lowest impact from multipath interference. This part must selected using the same window size for both the reference signal and the experimental signal. In this case, the size of three zero crossings of the experimental signals (see Fig. 4) is chosen (see Fig. 5). Notice that the transformed reference signal (blue) gives quite different shapes due to different τ_1 and κ values. The signal of the empty container is disturbed the most due to multipathing in the container walls.

C. Error Estimation

Using the system refractive index, temperature and mass of samples can be measured simultaneously; the volume can be measured before and after a heating cycle. The contributions to the errors in the measured quantities are summarized in Table I. The errors in n and κ can be converted to those for ε: $\Delta\varepsilon' = 2n\Delta n + 2\kappa\Delta\kappa$ and $\Delta\varepsilon'' = 2n\Delta\kappa + 2\kappa\Delta n$ [30].

The error in n is estimated to [30]

$$\Delta n = (n-1)\frac{\Delta d}{d} + \frac{c_0 \Delta\tau}{d} \tag{4}$$

TABLE I
UNCERTAINTY BUDGET FOR THE MEASURED QUANTITIES

Quanity	*Unit*	*Error*	*Uncer-tainty*	*Relative uncer-tainty (%)*
n	-	Propagation path	0.003-0.004	1.5
n	-	Measured delay	0-0.03	0-15
κ	-	Propagation path	0.0002-0.001	4
κ	-	Measured attenuation	0.005-0.25	10-75
m	kg	Mass of container	0.05	0.5-1
m	kg	Mass of sample	0.05	0.5-1
T	K	Probe temperature	1	0.4
T	K	Heterogenous heating	15	6
V	cm^3	Container dimension	60-70	2
V	cm^3	Calculated volume affected by upper surface definition	100-120	3

Uncertainty is connected to data intervals. Errors for n and k are based on measurements on small stones with minor multipathing and large stones with major multipathing. Errors in volume is based on two different container sizes $310 \times 410 \times 330$ mm^3 and $310 \times 310 \times 330$ mm^3.

where $\Delta\tau$ is the error in the determined time delay. It is caused by a resolution error, $\Delta\tau_r$, and an error due to frequency dependence of the losses of the investigated material, $\Delta\tau_f$

$$\Delta\tau = 2 \cdot \Delta\tau_r + \Delta\tau_f. \tag{5}$$

The error in the container thickness is estimated to $\Delta d = 1$ mm, which has been determined experimentally using a laser distance sensor to $\Delta\tau_r = 0.002$ns. The error $\Delta\tau_f = 0 - 0.03$ns and varies with the material investigated. There are two main contributions to $\Delta\tau_f$: first, the signal-to-noise ratio of the measured signal decreases with increasing κ, which results in larger $\Delta\tau_f$: second, the frequency dependence in (1) changes the waveform and hence affects the determined $\tau_1 - \tau_o$. The total error in n is, thus, $\Delta n = 0.003 - 0.034$ (see Table I).

The error in κ is estimated using [30]

$$\Delta\kappa = \kappa\frac{\Delta d}{d} + \kappa\frac{\Delta\alpha}{\alpha} \tag{6}$$

where $\alpha = -2\pi d\kappa/c_0$. The error in α and, hence, in κ varies with signal level and is also affected by interfering signals that may occur due to multipathing in heterogeneous materials. We estimate $\Delta\kappa = 0.0052 - 0.251$ for κ up to 0.06 (see Table I). This estimate is based on the change in the waveform between measurement on homogeneous and heterogeneous samples of the same type (here limestone gravel and larger limestones, respectively).

The mass scale that the heat-reaction chamber stands on has a calibrated accuracy of < 50 g. The total error of the mass is estimated to 0.1 kg (see Table I).

The temperature is measured both in the mineral compound and in the atmosphere inside the chamber, with the error of the temperature probes being 1 °C. The largest errors in relation to temperature measurement are connected to the acquisition of reliable temperatures of the mineral compound, which is estimated to an uncertainty of up to 15 °C. Larger containers with mineral compounds have longer temperature response time. The thermocouple is placed among the stones, not inside the stones. During heating, the mineral compound undergoes a chemical reaction that absorbs energy and counteracts the heating. The exterior of a stone may also be warmer than the interior. The total error of the temperature measurement is up to 16 °C (see Table I).

The uncertainty in volume is connected to the volume of the container and determination of the upper surface of the compound. The total error of the volume determination is estimated to 160–190 cm^3 (see Table I).

IV. MATERIAL PROPERTIES

We present results from experiments, in which calcination, i.e., production of burnt lime, was investigated. Burnt lime is used, e.g., in the steel industry, in the pulp industry, and for cleaning of water and flue gases. Freshwater was used as a reference material, but it is also of interest because it is physically and chemically bounded to the investigated limestone.

A. Water

Freshwater has well-known dielectric properties, which can be described by the Debye formula [31], [32]

$$\varepsilon(\omega, T) = \varepsilon_\infty(T) + \frac{\varepsilon_0(T) - \varepsilon_\infty(T)}{1 - i\omega\tau_{\text{rot}}(T)} \tag{7}$$

where ε_∞ and ε_0 are the optical and static permittivities, respectively, τ_{rot} is the rotational relaxation time, and ω is the angular frequency. The parameters of (7) can be modeled by

$$\varepsilon_0(T) = a_1 - b_1 T + c_1 T^2 - d_1 T^3 \tag{8}$$

$$\varepsilon_\infty(T) = \varepsilon_0(T) - a_2 e^{-b_2 T} \tag{9}$$

$$\tau_{rot}(T) = c_2 e^{\frac{d_2}{T + T_0}} \tag{10}$$

where $a_1 = 87.9144$, $b_1 = 0.404399$, $c_1 = 9.58726 \cdot 10^{-4}$, $d_1 = 1.32802 \cdot 10^{-6}$, $a_2 = 80.69715$, $b_2 = 4.415996 \cdot 10^{-3}$, $c_2 = 1.367283 \cdot 10^{-13}$, $d_2 = 651.4728$, $T_0 = 133.0699$, and T is the water temperature in °C.

B. Limestone and Burnt Lime

In the measurements limestones ($CaCO_3$) with the sizes of 16–32- and 40–80-mm stones were investigated. Since the stones are sifted, the specified figures are for the smallest parts of the stones. Thus, the stones of sizes 16–32 mm are never smaller than 16 mm, the smallest part of the stones is never larger than 32 mm, but the largest part can be greater than 32 mm; 40–80-mm stones are used in the production of burnt lime in lime shaft kilns. The used limestone consists of 96.5%–98% of $CaCO_3$. Other minerals are SiO_2, Al_2O_3, Fe_2O_3, MgO, and K_2O. Limestone ($CaCO_3$) decomposes into burnt lime (CaO) during heating: $CaCO_3$+ heat $\rightarrow$ CaO + CO_2. The used limestone is the type used in the production of burnt lime in industrial processes.

The chemical heat reaction of calcination is initiated at slow rate at +550 °C [33]. The decomposition temperature of $CaCO_3$ is reported to 890 °C–920 °C at CO_2 partial pressure of 1 bar [34]. The partial pressure of carbon dioxide (CO_2) influences the reaction rate. Lower pressure accelerates the heat reaction and higher pressure deaccelerates the reaction [35].

Limestone may have free and bound water inside the structure. Dehydration must be performed at +400 °C [36] to release the water of crystallization. Bound water will influence the dielectric properties. Therefore, the measurements of material compounds must consider drying of the medium before heating to temperatures, where the heat reaction starts.

V. Experimental Procedure and Results

In this section, we first present experimental results for n and κ versus temperature for freshwater to verify the measurement system and method for data analysis. Thereafter, we present results for the temperature and for n and κ from the calcination of limestone to burnt lime; finally, we present data for the n, κ, and mass versus time during calcination to illustrate the connection between radio and weight measurements.

A. Water

Freshwater was placed in a 32-L plastic container (interior measures: 367 × 267 mm). The starting temperature was +82 °C and the end temperature was +23 °C. The temperature was measured with a PT100 temperature sensor in the center of the container. The container was insulated with Styrofoam to make the cooling process slow. The water was cooled down for 44 h. The antenna housings were mounted on the short sides. Using the method described in Section III-B, n and κ were determined from the measured radio signals. In Fig. 7, the measured refractive index is shown with literature values [31], [32] obtained using (1)–(10). The frequency range was 0.85–2.65 GHz with an approximate center frequency of 1.67 GHz of the received signals. Thus, literature values are given for these frequencies.

The uncertainty in n is estimated to 1.5% and the uncertainty in κ is estimated to 20% (see Table I). This gives $\Delta n = 0.12 - 0.13$ and $\Delta\kappa = 0.04 - 0.06$.

Fig. 7 shows that our determined n and κ are in good agreement with literature data for freshwater, which corroborates that the presented measurement system and method for determining n and κ are reliable, with n being determined with significantly smaller relative errors.

B. Limestone and Burnt Lime

In the presented experiment, limestones of the size 16–32 mm were placed in a refractory container with the size of 310 × 310 × 330 mm (see Fig. 8). Thereafter, the container was placed in the heat-reaction chamber. One thermocouple was placed into the sample of limestones, and another was placed in the atmosphere of the heat-reaction chamber. The center frequency for this test was 2.5 GHz.

The investigated heating cycle was chosen to heat the stones slowly and to perform full calcination of the stones

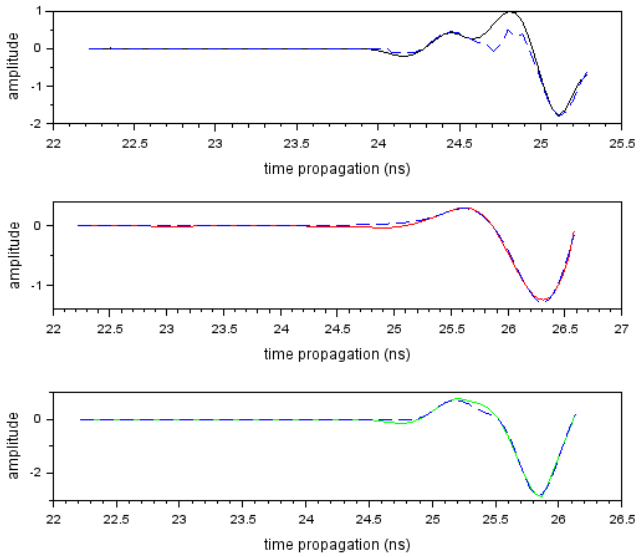

Fig. 6. Top: Reference signals $w(t)y_{0e}(t)$ (solid) and $w(t)y_{0c}(t)$ (dashed), where the latter is shifted τ_c and scaled (solid). Middle ($CaCO_3$) and bottom (CaO): Modeled, $z_m(t)$, (solid) and experimental, $z_x(t)$, (dashed) signals.

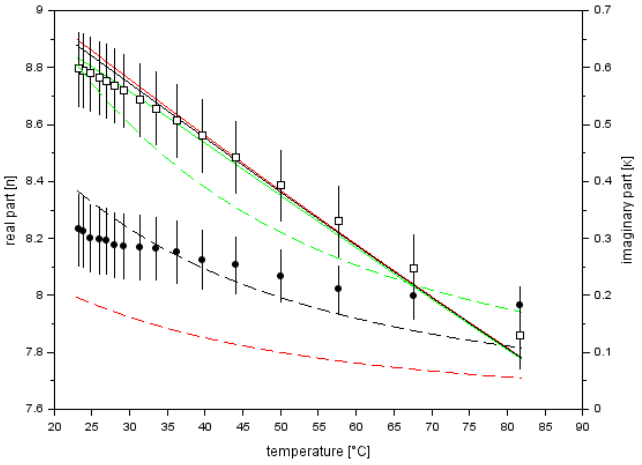

Fig. 7. Experimentally determined refractive index for water (open squares for real part and filled circles for imaginary part with error bars). Also shown are literature values for 0.85 GHz (red), 1.67 GHz (black), and 2.65 GHz (green). Real parts are drawn as full lines and imaginary parts as dashed lines.

(see Fig. 9). From the temperature measurements of the atmosphere and the limestones, the following were observed.

1) The limestones were dehydrated by heating to +450 °C and then cooling down to +200 °C. Dehydration shall be completed at +400 °C [36].
2) The heating cycle of the calcination starts at +200 °C and continues to +900 °C.
3) At temperatures above +550 °C, the $CaCO_3$ decarbonizes and begins to outgas CO_2 [33].
4) The limestones are at a constant temperature of +960 °C due to the ongoing endothermic chemical reaction. The temperature in the limestone and in the atmosphere is also different because limestone has longer temperature response time than the atmosphere.
5) At completed calcination, the temperature in the burnt lime is not suppressed and becomes gradually equal to the temperature in the atmosphere.

Fig. 8. Refractory container with a sample of limestones in a ceramic kiln.

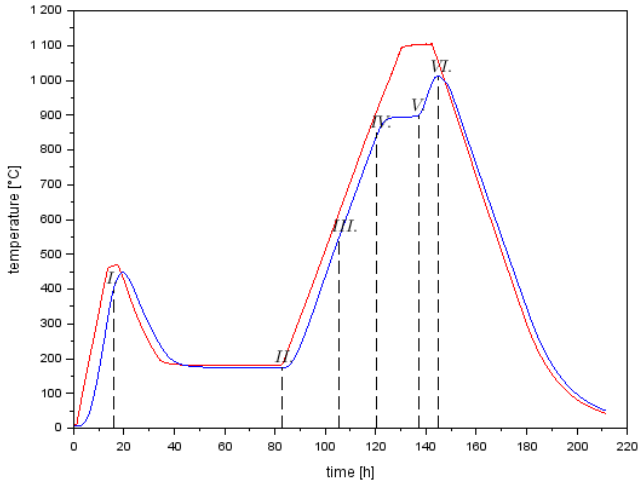

Fig. 9. Temperatures in the atmosphere (red) and in the investigated limestone (blue), with certain stages indicated: I. Dehydration of water completed. II. Heating cycle of calcination starts. III. Calcination starts. IV. Chemical process of calcination holds back temperature. V. Calcination finished. VI. Same temperature in the burnt lime and in the atmosphere.

6) When the calcination is finished, the temperature of the burnt lime becomes equal to the atmosphere temperature.

Measurements of n and κ were performed during the entire heating cycle every sixth second. The real and imaginary parts of the refractive index are plotted versus temperature in Fig. 10. The changes in material properties are clearly seen in the real part, n, and imaginary part, κ. Estimated errors for the real and imaginary parts are presented in Fig. 11.

In Fig. 10, the first part of the red curve for n between +200 °C and +550 °C shows the heating of $CaCO_3$. Here, n increases with temperature from 1.95 to 2.10. The data in Fig. 10 are for a density of approximately 1.5 gcm^{-3} (mixture of porous limestone and voids in-between stones). Literature

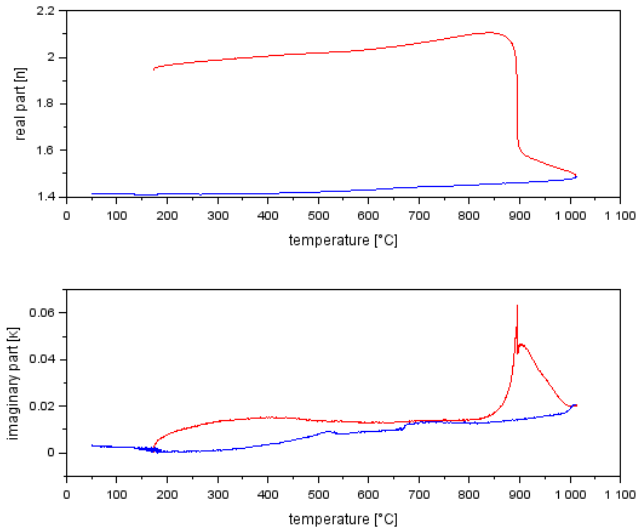

Fig. 10. Real n, (top) and imaginary parts, κ, of the mineral compound versus temperature, during heating (red) and cooling (blue).

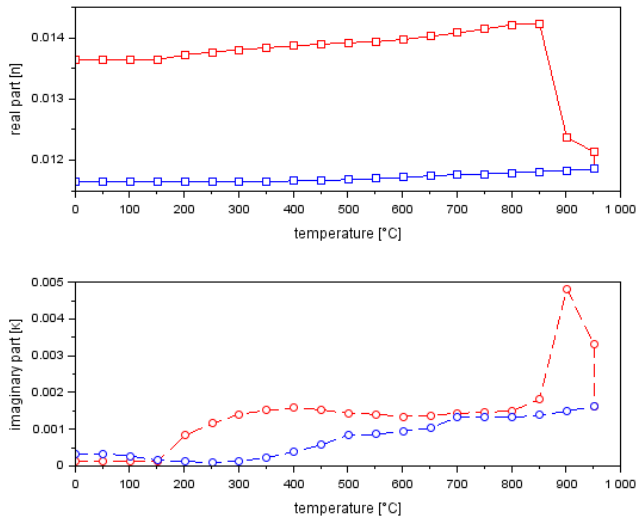

Fig. 11. Errors in the real n, (top) and imaginary parts, κ, of the mineral compound versus temperature, during heating (red) and cooling (blue).

values for limestone powder vary from $n = 1.6$ (for 1.0 gcm^{-3}) to $n = 2.5$ (for 2.6 gcm^{-3}) [37]. The room temperature data in Fig. 10 are, thus, in agreement with reported values.

Between +550 °C and +900 °C, there is a mixture of $CaCO_3$ and CaO. The peak in κ at +900 °C is explained by the decrease in bandgap with temperature and electrons being excited to the conduction band (see [38, Ch. 18.12]). At +900 °C, n decreases from $n = 2.0$ to $n = 1.6$; at this temperature, $CaCO_3$ is decomposed to CaO and CO_2. Above +900 °C, n is due to only to CaO. The blue line for n and κ in Fig. 10 corresponds to CaO cooling down to room temperature. Notice that $n = 1.4$ at room temperature, which is small compared to the literature value for CaO, which is of $n = 3.5$ at room temperature [39]. The data in Fig. 10 are for highly porous CaO, whereas the literature value is for bulk CaO.

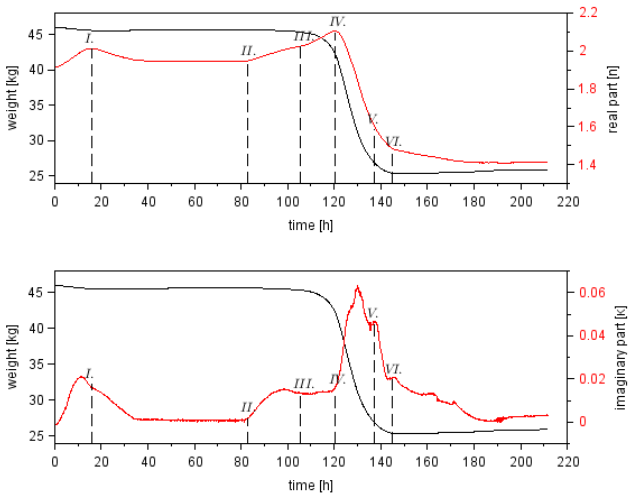

Fig. 12. Weight (blue, left y-axis) and refractive index (red, right y-axis) versus time during calcination. Upper figure shows the real part n and lower imaginary part, κ. Roman numerals are different stages (see Section V-B and V-C).

The errors in Fig. 11 vary strongly with temperature since the errors depend on the magnitude of n and κ. The relative errors are those in Table I.

C. Dielectric Properties and Mass

In Fig. 12 n, κ, and the mass are shown versus time during calcination. The different stages of the heating cycle (roman numerals in Fig. 9) are indicated. Comparing Fig. 12 with Fig. 9, we can interpret the changes in n, κ, and mass with time as follows.

1) n and κ increase and the mass decreases slightly until the temperature has reached +400 °C due to dehydration.
2) n is relatively constant, κ increases slightly, and the mass is relatively constant when the temperature starts to increase.
3) n increases with temperature, κ has reached a constant level, and the mass is relatively constant before calcination starts.
4) The increase in n accelerates with temperature, while the mass loss is accelerating during calcination (CO_2 is emitted); thereafter, n reaches a maximum when the temperature is constant during the endothermic reaction; κ starts to increase at the peak in n and the mass starts to decrease.
5) The mass and n decrease jointly during calcination, and κ reaches a peak before it starts to decrease.
6) The change in mass is relatively small and n and κ decrease slowly after full calcination. At lower temperatures, hydration and recarbonization can be observed as the mass increases slightly.

Notice that the ratio between initial mass (at II in Fig. 12) and lowest mass (at VI in Fig. 12) is 56%. Thus, all $CaCO_3$ has been decomposed to CaO and CO_2 since the ratio of the molar masses is 56%; $CaCO_3$ has a molar mass of 100.0869 and CaO has 56.0774. The mass of CO_2 is not measured by the scale.

VI. Discussion

The presented system was designed for the simultaneous measurement of microwave properties, mass, and temperature. Its performance is therefore not as good as dedicated instruments for separate measurements. The determination of n and κ is affected by multipathing. This effect could be reduced by not using a container, but the highly corrosive CaO-dust degenerated the heating elements quickly in the kiln. Antennas with higher directivity and improved shielding with radar absorbing materials could possibly reduce the effects of multipathing. An even larger kiln would possibly reduce the problem, but it was not available.

The signal-to-noise ratio of the measured signals is in practice much lower than the 70 dB caused by the transmitter and receiver. In practice, interference from multipathing results in significantly higher numbers. Multipathing depends on the structure of the investigated material compounds and the used container.

The real part, n, can be determined with relatively high accuracy. It is determined from time delays that can be measured with high accuracy, in particular for the narrow pulses of the UWB signals using windowing that suppresses interfering signals from multipathing. In frequency domain techniques (e.g., using measured S-parameters), this type of suppression of noise and interference is not straightforward. The determined imaginary part, κ, depends on the shape of the measured signal, and it is therefore more sensitive to noise and interference and the windowing also affects it more than n.

The determined complex refractive index and the errors can be presented as permittivity (see Section III) in order to make a comparison with other techniques easy. Using the data in Table I, we get that $\Delta\varepsilon'/\varepsilon'$ is 3%–30% and $\Delta\varepsilon''/\varepsilon''$ is 20%–150%. These errors are relatively high when compared to conventional methods at approximately the same frequencies; for cavity methods, typical numbers reported are $\Delta\varepsilon'/\varepsilon'$ 2%–3% [40], 5%–8% [40], and 0.4%–2% [41]; typical numbers for $\Delta\varepsilon''/\varepsilon''$ are 6%–9% [40], 14%–22% [40], and 10%–50% [41]. For waveguide methods, typical numbers are for $\Delta\varepsilon'/\varepsilon'$ 1.7% [42] and 5% [43]; for $\Delta\varepsilon''/\varepsilon''$ 37% [42] and 15% [43] are examples. Thus, the presented technique gives larger errors than cavity and waveguide techniques; the advantage is the use of large sample volumes and the simultaneous heating, temperature, and mass measurement.

The heating cycle must be designed for the investigated material. The temperature response time of the investigated material and the expected heat reaction must be considered. The heating cycle must also be chosen to obtain reliable temperature measurements. Too fast heating and cooling may damage the containers and the kiln. Several tests are therefore made before a suitable heating cycle is found for a specific material.

The large heat-reaction chambers (see Fig. 1) compared to smaller chambers have the advantage that materials used in industrial production material (for example, larger stones) can be investigated under conditions similar to those in full-size industrial kilns. Thermogravimetric measurements may also depend on the investigated volume [22]; our results may be closer to those in a production environment.

Our goal is to develop a real-time control of industrial lime shaft kilns, where the temperature and the calcination are determined in-line. The developed heat-reaction chamber

is an important equipment to get data for different limestone qualities and different stone sizes. In the future, implementation and measurements shall be carried out in an industrial facility. In a production environment, placement and number of sensors may be changed.

The presented measurement system could be used to study heat reactions of different mineral compounds, such as limestone, hot meal (the mineral mixture of limestone, sand, and clay for the production of cement), kiln refractories, and ceramic fibers. It will be used for future studies of other mineral compounds.

The type of measurements that now can be made makes it possible also to perform studies, where chemical reaction kinetics, based on thermogravimetric data analysis, is combined with modeling of permittivity of heterogenous materials using, e.g., effective medium approximations (see [44]). We intend to develop a model that converts dielectric measurements into temperature and calcination level in the production of kilns for burnt lime.

VII. Conclusion

A measurement system for the simultaneous measurement of dielectric properties, mass, and temperature of mineral compounds at high temperatures has been developed. The purpose is to study how the changes in dielectric properties with temperature are related to the change in mass with temperature; the change in mass is affected by chemical processes like dehydration and calcination. Samples of volumes in the range of 0.01–0.1 m^3 can be investigated at temperatures from room temperature up to +1000 °C. The possible volumes enable measurements on heterogenous samples and make the conditions similar to those in industrial applications compared to instruments, where smaller volumes are used. Previously reported measurement systems for high temperatures, e.g., [12] and [13], use volumes of a few cubic centimeters and without the possibility of simultaneous mass measurement.

The system uses UWB radio signals, which is suitable in the system, where tradeoffs had to be made between the different measurement systems. A dedicated method to determine n and κ from measured radio signals has been used. Good agreement was found between experimental data for n and κ for water and literature values. The errors in the determined n and κ are somewhat larger than in system dedicated to measure only dielectric properties.

Experimental data for calcination, where $CaCO_3$ is decomposed to CaO and CO_2 during heating, as a function of time, were presented. The calcination is clearly seen both as a change in mass and as changes in n and κ. Dehydration at lower temperatures was observed both as a change in mass and in n and κ. The presented measurement system is an important step toward systems for monitoring calcination of large quantities of limestone in industrial applications using UWB radio techniques.

References

[1] L. Zhou, Z. Liu, L. Tang, and Y. Pei, "Design and characterization for a high-temperature dual-band radome wall structure for airborne applications," *Mater. Des.*, vol. 114, pp. 264–270, Jan. 2017.

[2] C. H. Mueller and F. A. Miranda, "High temperature permittivity measurements of alumina enhanced thermal barrier (AETB-8) material for CEV antenna radomes," in *Proc. IEEE Antennas Propag. Soc. Int. Symp.*, Jul. 2010, pp. 1–4.

[3] Y. Yu, B. Han, and F. Xia, "PDC-SiAlCN ceramic based wireless passive temperature sensors using integrated resonator/antenna up to 1100 °C," *Sensor Rev.*, vol. 40, no. 1, pp. 62–70, Jan. 2020.

[4] L. Wu, Y. Zhang, F. Wang, W. Ma, T. Xie, and K. Huang, "An on-line system for high temperature dielectric property measurement of microwave-assisted sintering materials," *Materials*, vol. 12, pp. 665–676, Feb. 2019.

[5] B. Garcia-Baños, J. Catalá-Civera, F. Peñaranda-Foix, P. Plaza-González, and G. Llorens-Vallés, "In situ monitoring of microwave processing of materials at high temperatures through dielectric properties measurement," *Materials*, vol. 9, no. 5, p. 349, May 2016.

[6] S. Soldatov, M. Umminger, A. Heinzel, G. Link, B. Lepers, and J. Jelonnek, "Dielectric characterization of concrete at high temperatures," *Cement Concrete Compos.*, vol. 73, pp. 54–61, Oct. 2016.

[7] A. Nesbitt et al., "Development of a microwave calorimeter for simultaneous thermal analysis, infrared spectroscopy and dielectric measurements," *Meas. Sci. Technol.*, vol. 15, no. 11, pp. 2313–2324, Nov. 2004.

[8] A. A. Salema, F. N. Ani, J. Mouris, and R. Hutcheon, "Microwave dielectric properties of Malaysian palm oil and agricultural industrial biomass and biochar during pyrolysis process," *Fuel Process. Technol.*, vol. 166, pp. 164–173, Nov. 2017.

[9] D. Vaccaneo, L. Sambuelli, P. Marini, R. Tascone, and R. Orta, "Measurement system of complex permittivity of ornamental rocks in L frequency band," *IEEE Trans. Geosci. Remote Sens.*, vol. 42, no. 11, pp. 2490–2498, Nov. 2004, doi: 10.1109/TGRS.2004.835225.

[10] V. L. Mironov and Y. I. Lukin, "Temperature dependable microwave dielectric model for frozen soils," *PIERS Online*, vol. 5, no. 5, pp. 406–410, 2009.

[11] M. A. C. W. D. Silveira, J. A. M. D. Luz, G. L. D. Faria, and F. M. P. Coutinho, "Calcination thermokinetics of three Brazilian limestones," *Cerâmica*, vol. 66, no. 379, pp. 297–306, Sep. 2020, doi: 10.1590/0366-69132020663792910.

[12] R. Behrend, B. Garcia-Banos, V. Uhlig, H. Krause, and J. M. Catala, "Dielectric characterization of raw materials at high temperatures," *Process Eng.*, vol. 93, nos. 6–7, pp. E63–E69, 2016.

[13] J. M. Catalá-Civera, A. J. Canós, P. Plaza-González, J. D. Gutiérrez, B. García-Baños, and F. L. Peñaranda-Foix, "Dynamic measurement of dielectric properties of materials at high temperature during microwave heating in a dual mode cylindrical cavity," *IEEE Trans. Microw. Theory Technol.*, vol. 63, no. 9, pp. 2905–2913, Sep. 2015.

[14] Y. Zhang, E. Li, J. Zhang, C. Yu, H. Zheng, and G. Guo, "A broadband variable-temperature test system for complex permittivity measurements of solid and powder materials," *Rev. Sci. Instrum.*, vol. 89, no. 2, Feb. 2018, Art. no. 024701.

[15] C. Larsson, D. Sjøberg, and L. Elmkvist, "Waveguide measurements of the permittivity and permeability at temperatures of up to 1000 °C," *IEEE Trans. Instrum. Meas.*, vol. 60, no. 8, pp. 2872–2880, Aug. 2011.

[16] A. E. Bogle, M. W. Hyde, M. J. Havrilla, and J. S. Sovern, "High-temperature RF material characterization using a dual-chambered rectangular waveguide fixture," *IEEE Trans. Instrum. Meas.*, vol. 66, no. 9, pp. 2422–2427, Sep. 2017.

[17] V. V. Varadan and L. Ji, "Temperature dependence of resonances in metamaterials," *IEEE Trans. Microw. Theory Techn.*, vol. 58, no. 10, pp. 2673–2681, Oct. 2010.

[18] H. Chen et al., "An improved NRW method for thin material characterization using dielectric filled waveguide and numerical compensation," *IEEE Trans. Instrum. Meas.*, vol. 71, pp. 1–9, 2022, doi: 10.1109/TIM.2021.3129205.

[19] Q. Shi, Q.-X. Chu, M.-Z. Xiao, F.-C. Chen, X.-Q. Huang, and X. He, "Complex permittivity measurement utilizing multiple modes of a rectangular cavity," *IEEE Trans. Instrum. Meas.*, vol. 72, pp. 1–8, 2023, doi: 10.1109/TIM.2022.3225926.

[20] K. M. Hock, "Error correction for diffraction and multiple scattering in free-space microwave measurement of materials," *IEEE Trans. Microw. Theory Techn.*, vol. 54, no. 2, pp. 648–659, Feb. 2006, doi: 10.1109/TMTT.2005.862666.

[21] J. G. Dunn, "Thermogravimetry," in *Encyclopedia of Analytical Chemistry*, R. A. Meyers and D. Dollimore, Eds. Hoboken, NJ, USA: Wiley, 2006, doi: 10.1002/9780470027318.a6605.

[22] N. Saadatkhah et al., "Experimental methods in chemical engineering: Thermogravimetric analysis—TGA," *Can. J. Chem. Eng.*, vol. 98, no. 1, pp. 34–43, Jan. 2020.

[23] B. García-Baños, J. M. Catalá-Civera, J. R. Sánchez, L. Navarrete, A. M. López-Buendía, and L. Schmidt, "High temperature dielectric properties of iron- and zinc-bearing products during carbothermic reduction by microwave heating," *Metals*, vol. 10, no. 5, p. 693, May 2020.

[24] P. Ottoson, D. Andersson, and D. Rönnow, "UWB radio measurement and time-domain analysis of anisotropy in wood chips," *IEEE Sensors J.*, vol. 18, no. 22, pp. 9112–9119, Nov. 2018.

[25] V. Choudhary and D. Rönnow, "A nondestructive testing method for the determination of the complex refractive index using ultra wideband radar in industrial applications," *Sensors*, vol. 20, no. 11, p. 3161, Jun. 2020, doi: 10.3390/s20113161.

[26] P. Ottosson, F. Blomqvist, D. Andersson, and T. Ekman, "Heat transfer modelling and adjustment from radar measurements in reheating steel furnaces," in *Proc. AISTech*, Nashville, TN, USA, 2021, pp. 1725–1741.

[27] P. Ottosson. (2020). *Radar and Radio Measurement Sensors and Antennas*. [Online]. Available: https://www.radarbolaget.com/products/sensor-antennas

[28] J. Sachs, "M-sequence ultra-wideband-radar: State of development and applications," in *Proc. Int. Conf. Radar*, 2003, pp. 224–229, doi: 10.1109/RADAR.2003.1278743.

[29] O. Javashvili and D. Andersson, "New method for design implementation of Vivaldi antennas to improve its UWB behaviour (EuCAP 2010)," in *Proc. 4th Eur. Conf. Antennas Propag.*, Barcelona, Spain, 2010, pp. 1–5.

[30] D. Rönnow, P. Ottosson, and D. Andersson, "Microwave complex permittivity and anisotropy of conifer wood chips vs moisture content: Experiments and modeling," *J. Wood Sci.*, vol. 68, no. 1, p. 22, Dec. 2022.

[31] W. J. Ellison, "Permittivity of pure water, at standard atmospheric pressure, over the frequency range 0–25THz and the temperature range 0–100 °C," *J. Phys. Chem. Reference Data*, vol. 36, no. 1, pp. 1–18, Mar. 2007.

[32] J. Hamelin, J. Mehl, and M. Moldover, "The static dielectric constant of liquid water between 274 and 418 K near the saturated vapor pressure," *Int. J. Thermophys.*, vol. 19, no. 5, pp. 1359–1380, 1998.

[33] N. Curetti et al., "Thermal stability of calcium oxalates from CO_2 sequestration for storage purposes: An in-situ HT-XRPD and TGA combined study," *Minerals*, vol. 12, no. 1, p. 53, Dec. 2021, doi: 10.3390/min12010053.

[34] M. Silva, E. Specht, and J. Schmidt, "Thermophysical properties of limestone as a function of origin (part 2): Calcination enthalpy and equilibrium temperature," *ZKG Int.*, vol. 6, pp. 51–57, Jan. 2010.

[35] J. M. Valverde, P. E. Sanchez-Jimenez, and L. A. Perez-Maqueda, "Limestone calcination nearby equilibrium: Kinetics, CaO crystal structure, sintering and reactivity," *J. Phys. Chem. C*, vol. 119, no. 4, pp. 1623–1641, 2015.

[36] J. Ihli et al., "Dehydration and crystallization of amorphous calcium carbonate in solution and in air," *Nature Commun.*, vol. 5, no. 1, Jan. 2014, Art. no. 3169, doi: 10.1038/ncomms4169.

[37] C. T. Dervos, J. A. Mergos, and A. A. Iosifides, "Characterization of insulating particles by dielectric spectroscopy: Case study for $CaCO_3$ powders," *Mater. Lett.*, vol. 59, no. 22, pp. 2842–2849, 2005.

[38] W. D. Callister, *Materials Science and Engineering: An Introduction*. New York, NY, USA: Wiley, 2007.

[39] M. A. Subramanian, R. D. Shannon, B. H. T. Chai, M. M. Abraham, and M. C. Wintersgill, "Dielectric constants of BeO, MgO, and CaO using the two-terminal method," *Phys. Chem. Minerals*, vol. 16, pp. 741–746, Nov. 1989.

[40] A. K. Jha and M. J. Akhtar, "A generalized rectangular cavity approach for determination of complex permittivity of materials," *IEEE Trans. Instrum. Meas.*, vol. 63, no. 11, pp. 2632–2641, Nov. 2014, doi: 10.1109/TIM.2014.2313415.

[41] A. Kik, "Complex permittivity measurement using a ridged waveguide cavity and the perturbation method," *IEEE Trans. Microw. Theory Techn.*, vol. 64, no. 11, pp. 3878–3886, Nov. 2016, doi: 10.1109/TMTT.2016.2614509.

[42] Y. Kato, M. Horibe, M. Ameya, S. Kurokawa, and Y. Shimada, "New uncertainty analysis for permittivity measurements using the transmission/reflection method," *IEEE Trans. Instrum. Meas.*, vol. 64, no. 6, pp. 1748–1753, Jun. 2015, doi: 10.1109/TIM.2015.2401231.

[43] C. M. A. Niamien, "Unique-solution single-sample complex dielectric characterization through linear phase approximation," *IEEE Open J. Antennas Propag.*, vol. 3, pp. 475–487, 2022, doi: 10.1109/OJAP.2022.3170790.

[44] A. H. Sihvola, *Electromagnetic Mixing Formulas and Applications*. London, U.K.: Institution of Electrical Engineers, 1999.

Patrik Ottosson received the M.Sc. degree in photogrammetry and geodesy and the Ph.D. degree in geoinformatics from the KTH Royal Institute of Technology, Stockholm, Sweden, in 1991 and 2001, respectively.

He is currently the Managing Director at Radarbolaget, Gävle, Sweden, and a Lecturer at the University of Gävle, Gävle. Radarbolaget develops UWB radar and radio measurement system and new technological solutions for moist wood measurement at district heating plants and at pulp plants, calcination measurement in lime shaft kilns, and high-accuracy radar system for steel expansion measurements in reheating furnaces.

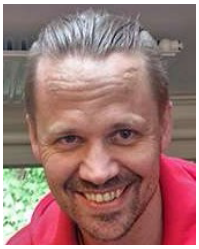

Daniel Andersson received the B.Sc. degree in electronics from the University of Gävle, Gävle, Sweden, in 2000.

He is currently a Developer of radar systems and radar solutions at Radarbolaget, Gävle. He is the inventor of the highly accurate UWB radar and radio measurement system used for this article.

Vipin Choudhary (Member, IEEE) received the M.Tech. and Licentiate degrees in electronics and electrical engineering from Amity University, Noida, Uttar Pradesh, India, and the KTH Royal Institute of Technology, Stockholm, Sweden, in 2017 and 2021, respectively. He is currently pursuing the Ph.D. degree in electrical engineering with the University of Gävle, Gävle, Sweden, with a focus on RF and antenna measurements, nondestructive testing, radar measurements, radar imaging, microwave/radar absorbers materials, SAR, polarimetry measurements, RF measurement techniques, and signal processing.

Daniel Rönnow (Member, IEEE) received the M.Sc. degree in engineering physics and the Ph.D. degree in solid state physics from Uppsala University, Uppsala, Sweden, in 1991 and 1996, respectively.

He is currently a Professor at the University of Gävle, Gävle, Sweden.